KLOE-2

The KLOE-2 Collaboration

D. Babusci, G. Bencivenni, C. Bloise, F. Bossi, G. Capon (Ass.), P. Ciambrone,
F. Curciarello (PostDoc), E. Dané (Art. 23), E. De Lucia (Resp.), A. De Santis (Art.36),
P. De Simone, D. Domenici, G. Felici, P. Fermani (PostDoc), G. Fortugno (Tec.), S. Giovannella,
M. Martini (Ass)*, S. Miscetti, E. Perez del Rio (PostDoc), P. Santangelo, I. Sarra (PostDoc),
F. Sborzacchi (Tec.), M. Silarski (PostDoc), G. Venanzoni.

In collaboration with "LNF-SEA"
P. Albicocco, A. Balla, M. Beretta, M. Carletti, S. Ceravolo, G. Corradi, U. Denni, A. Frani,
M. Gatta, R. Lenci, G. Papalino, B. Ponzio

*Also Dipartimento di Scienze e Tecnologie applicate,"Guglielmo Marconi" University, Rome, Italy

1   DAΦNE Operation and KLOE-2 Run

During 2016 both KLOE-2 and DAΦNE have been smoothly operated and Data taking has been progressing as expected. Run-II started in November 2015 aiming at a total delivered luminosity of 2.5 fb^{-1} by July 2016, an intermediate milestone which has been met and also overcome as shown in Fig. 1. Run-III started in September 2016 and ∼3 fb^{-1} total integrated luminosity has been acquired by December 2016.
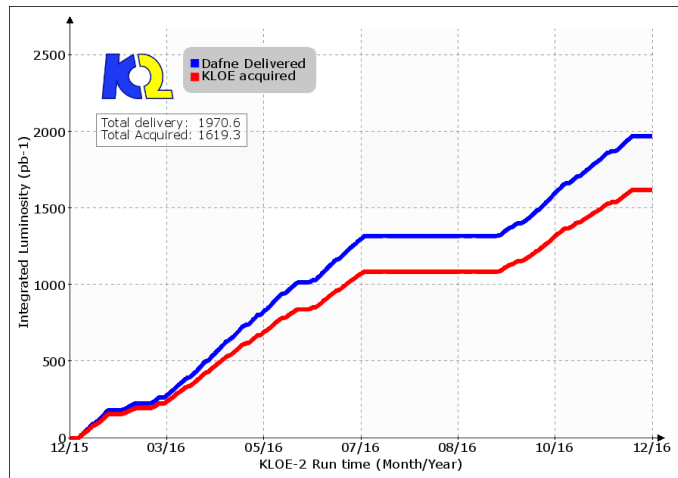

Figure 1: 2016 Integrated luminosity: the blue curve shows DAΦNE delivered luminosity and the red curve KLOE-2 acquired luminosity respectively.

2   Detector Operation

For e$^+$e$^-$ injection optimization and to guarantee good data quality and safely operate all KLOE-2 sub-detectors, the information from three indicators of the machine background level is sent on-line

to DAΦNE operators: the current measured on the first Inner Tracker (IT) layer, the total current measured in the Drift Chamber (DC) and the background level measured in the Electromagnetic Calorimeter (EMC) end-caps. DC and EMC have been operating steadily and with expected performance.

The Inner Tracker has been equipped with a new HV system with active voltage dividers to cope with present running conditions. The first set of alignment and calibration parameters has been used with Bhabha scattering events to validate the integrated tracking using both DC and IT information with a Kalman filter technique. The IT+DC track reconstruction has been integrated with a revised vertexing algorithm in the official reconstruction and an improved vertex resolution with respect to the DC tracking only has been measured with $\rho - \pi$ decays.

The π^0 production from $\gamma\gamma$ scattering is tagged by the coincidence between one or both HET stations, and the KLOE calorimeter, when two clusters are reconstructed. The search for π^0 production is ongoing with 550 pb^{-1} of KLOE-2 data. KLOE calorimeter energy, momentum and time resolution for 70 MeV photons have been measured for signal simulation and for signal/background separation.

3 Data Quality and Analysis

Event Classification Counters are constantly monitored to provide fast feedback during data taking. To assess data quality in 2016 several benchmark channels have been reconstructed and analyzed. Fully neutral processes like $\phi \to \eta\gamma$, with both $\eta \to 3\pi^0$ and $\eta \to \gamma\gamma$, have been used to monitor the EMC performance. The comparison of the distribution of the angle between photon pairs and of the photon energy after the kinematic fit is shown in fig.2.
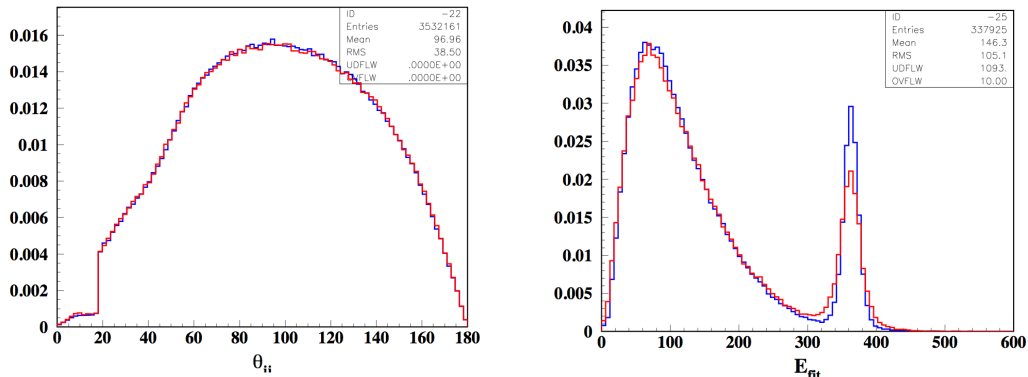

Figure 2: $\phi \to \eta\gamma$, with $\eta \to 3\pi^0$, comparison of 2016 (red) with the old KLOE data (blue).

Decays with charged secondaries like $K_{L,S} \to \pi^+\pi^-$ have been used to monitor the tracking performance. As an example fig.3 shows the K_S lifetime obtained with 2016 data compared with old (2005) KLOE data. The measured lifetimes, in τ_S units, resulting from the fit to the K_S decay time distributions are in good agreement.

An energy scan has been performed in April by changing DAΦNE radio-frequency value to find the best working point for the experiment (fig.4-left). The ϕ-meson line shape has been obtained with $\phi \to K_S K_L$ with $K_S \to \pi^+\pi^-$ and $\phi \to \eta\gamma$ with $\eta \to 3\pi^0$ and $\eta \to \gamma\gamma$ (fig.4-right). The number of events has been normalized to very large angle Bhabha scattering events, and the fit has been performed by including radiative corrections and beam energy spread (300 keV) in the
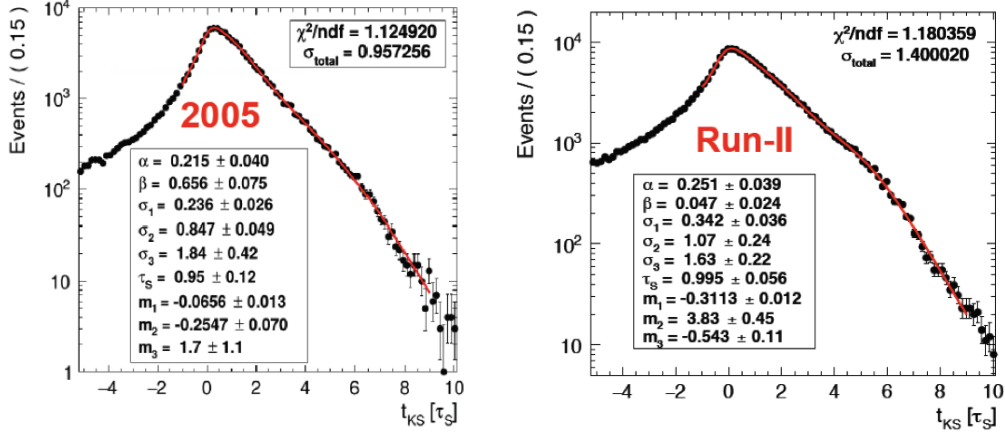
Figure 3: Comparison of K_S decay time distribution: left 2005 data and right Run-II 2016 data.

line shape. To run exactly at the ϕ-meson peak, DAΦNE center of mass energy has been shifted by +550 keV.
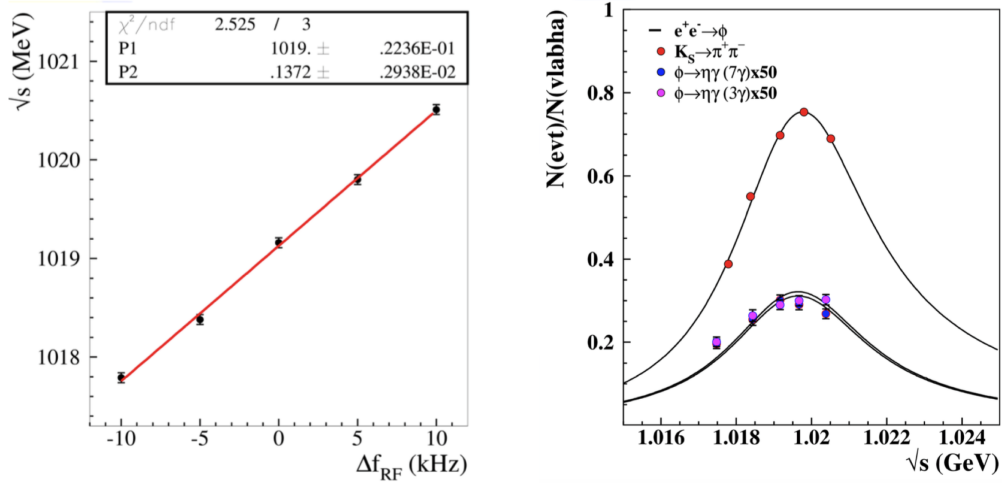

Figure 4: Left: $\sqrt{s}$ vs DAΦNE radio frequency shift. Right: ϕ-meson line shape.

A first look at $K_S \to 3\pi^0$ decay has been given with the new data: about 20 pb^{-1} have been analyzed by selecting events with a K_L interacting in EMC and at least three prompt photons. $K_S \to 2\pi^0$ events have been used as normalization sample. The same analysis strategy used with the old KLOE analysis has been applied. The old analysis was based on 1.7 fb^{-1} and set the best upper limit at present: $Br(K_S \to 3\pi^0) < 2.6 \times 10^{-8}$ at 90% C.L.. At the end of the analysis chain zero signal events have been selected, corresponding to an upper limit of $O(10^{-6})$. Optimization of selection criteria is ongoing to cope with increased background with respect to KLOE data.

4 CED

In 2016 KLOE computing architecture has changed completely the data handling paradigm. Our latest effort to increase the performance of data-taking machines and the number of processes running simultaneously has passed through the implementation of the GPFS protocol. We have taken over the NFS communication protocols with the GPFS data and file systems handling protocol. This change required also an architectural change we had already made to improve the NFS server architecture. The old architecture with two huge servers managing all files produced and processed from the experiment, has been changed with a new peer servers architecture where the handling of the files is demanded, logically to the GPFS and physically to the Storage Area Network. Every component of the experiment, DAQ, tape servers, DB server, CPU bound server, interactive servers, manage its own data with the assistance of GPFS lightweight server, through San Storage Area Network. Performance increased by factor ten together with a cost reduction because the hardware used for Storage Area Network is less expensive than TenGigabit Ethernet hardware. The servers have become more light and are now a small fraction of a partitionable Power architecture computer. Moreover the servers are dynamically located on a bigger machine which uses the most part of it as CPU bound server.

4.1 DAQ

Previously NFS protocols used an Ethernet connection to deliver files to tape drive server, sharing the bandwidth with the Data Taking Process. Now with GPFS, the tape drive server reads the files to be stored directly from SAN disk arrays, without disturbing the DAQ processes. The tape servers read and write data from the tape library without serving any of those data files to other tasks. Each client uses the SAN architecture and the GPFS protocol to read and write files back and forth on the disk arrays without asking nothing more than the lock to the GPFS servers.

4.2 Data Servers

We no longer need a huge server with many PCI cards and a lot of memory to face the clients requests. The servers now are the smallest partition on the cluster. The fraction of CPU dedicated to service tasks decreased dramatically. Due to the fact that any process reads and writes its own data asking to the GPFS server only the permission to open the files, the number of reconstruction program running simultaneously has increased from 120 to 320, saturating our CPU available but not the data bandwidth we gain with the new architecture. If we had others usable CPUs for data reconstruction, the number of runs could increase to 860 before saturating the actual bandwidth.

4.3 New disk array

The new 900 TB disk array allows the number of cartridges mounts on the tape libraries to be reduced. The users' programs can access and analyze a huge amount of files for days, without losing the recalled files due to another user request and with no impact on the space needed for the data reconstruction and MC production. The buffer throughput is about three Gigabyte per second, enough to feed twice the number of machines in the cluster.

5 Physics achievements

More stringent limits on the U-boson searches in the dark sector have been set in the $\rho - \omega$ region and above with the $e^+e \to U\gamma, U \to \pi^+\pi$ continuum process [1]. Some light has been shed on the discrepancy between experimental results and theoretical predictions from Vector Dominance

Model in conversion decays, performing the first measurement of the transition form factor $F_{\phi\pi^0}(q^2)$ and significantly improving the determination of the branching ratio of with $\phi \to \pi^0 e^+ e$ [2]. The Dalitz plot distribution for the $\eta \to \pi^+\pi^-\pi^0$ decay has been studied with the world's largest sample, improving the statistical uncertainty on all parameters by a factor two [3]. The first measurement of $\alpha(s)$ running in the time-like region $0.6 < \sqrt{s} < 0.975$ GeV has been performed showing more than 5σ significance of the hadronic contribution to the running of $\alpha(s)$. It represents the strongest direct evidence both in time- and space-like regions achieved in a single measurement and the first measurement of both real and imaginary part of $\Delta\alpha(s)$ [4].

5.1 Limit on the production of a new vector boson in $e^+e \to \gamma, U \to \pi^+\pi$ with the KLOE experiment

KLOE searched for a short lived dark photon decaying to $\pi^+\pi^-$ by looking for a resonant peak in the dipion invariant mass spectrum with initial-state radiation (ISR) $\pi^+\pi^-\gamma$ events [1]. The search for $U \to \pi^+\pi^-$ events has been applied to an integrated luminosity of 1.93 fb^{-1}, selecting events with a small angle ISR photon and two charged tracks with acceptance between $50°$ and $130°$. Kinematical cuts and the small angle event selection allowed to reduce the background coming from Final State Radiation and ϕ-resonant processes and to increase sensitivity to the dark photon decay. At the end of the analysis chain residual backgrounds from $e^+e^- \to \phi \to \pi^+\pi^-\pi^0$ and $e^+e^- \to \ell^+\ell^-\gamma$ ($\ell = e, \mu$) ISR processes still survive at the level of few %.

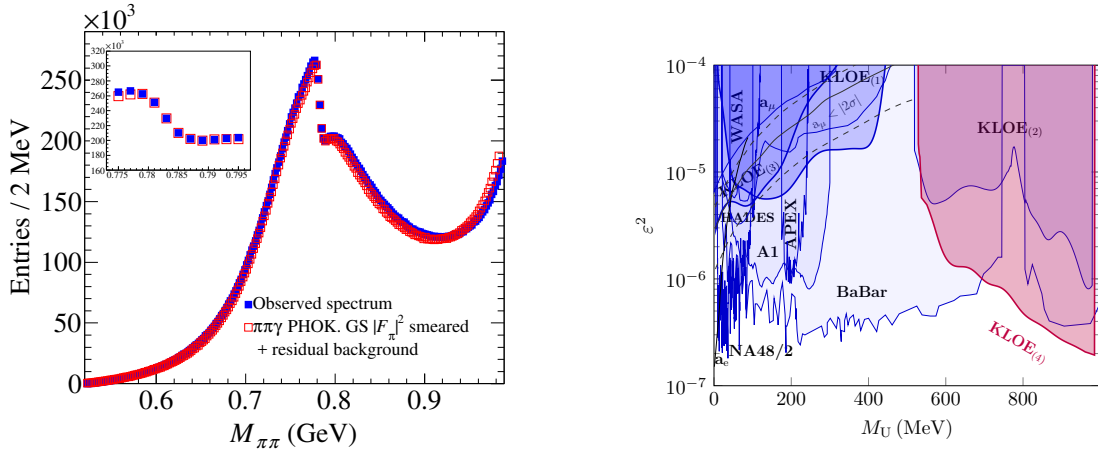Figure 5: Left: Invariant mass distribution for the $e^+e^- \to U\gamma$, $U \to \pi^+\pi^+$ process, compared with PHOKHARA MC expectation. Right: 90% CL exclusion plot for ε^2 as a function of the U boson mass (KLOE$_{(4)}$) together with KLOE limits from ϕ Dalitz decay (KLOE$_{(1)}$), $e^+e^-\gamma$ (KLOE$_{(3)}$), $\mu^+\mu^-\gamma$ (KLOE$_{(2)}$) and exclusion plots from other experiments. The solid lines are the limits from the muon and electron anomaly. The gray line shows the U boson parameters that could explain the observed a_μ discrepancy with a 2σ error band (gray dashed lines).

No significant dark photon signature has been observed in the $M_{\pi\pi}$ spectrum and a limit at 90% C.L. has been extracted on the number of events by means of the CL$_S$ technique. The irreducible background $e^+e^- \to \pi^+\pi^-\gamma$ has been estimated directly from data with a fit to the side bands with Chebyshev polynomials. In the $\rho - \omega$ region, where the fit is not possible, its contribution has been evaluated by using PHOKHARA MC generator (inset of Fig. 5-left) smeared with detector invariant mass resolution (about 2 MeV). Fig. 5-right shows the limit extracted on

the mixing strength ε^2, after a smoothing, in comparison with limits from other experiments in the mass range 0–1 GeV. The limit takes into account systematic errors due to the evaluation of the irreducible background and to the extraction formula ($\leq 1\%$). The 90% CL upper limit on ε^2 reaches a maximum value of 1.82×10^{-5} at 529 MeV and a minimum value of 1.93×10^{-7} at 985 MeV, improving current limits in the explored region.

5.2 Measurement of the $\phi \to \pi^0 e^+ e$ transition form factor with the KLOE detector

Vector Meson Dominance (VMD) model fails to describe the vector to pseudoscalar transition form factor (TFF) for the process $\omega \to \pi^0 \mu^+ \mu^-$, as measured by the NA60 collaboration [5]. New measurements of $VP\gamma^*$ transitions are therefore needed to confirm this evidence. A detailed study of the $\phi \to \eta e^+ e^-$ and $\phi \to \pi^0 e^+ e^-$ decays has been performed with 1.7 fb^{-1} of KLOE data [6, 2].

No data are available on the transition form factor of the $\phi \to \pi^0 e^+ e^-$ decay. A large background contamination is still present after preselection cuts, requiring two tracks and two photon candidates in the final state. Dedicated analysis cuts strongly reduce the main background component of Bhabha scattering events to $\sim 20\%$, which dominates for $M_{ee} > 300$ MeV (Fig. 6-left). The other residual relevant background contribution is from ϕ-meson radiative decays. At the end of the analysis, about 14,500 events are selected, with a total background contamination of $\sim 30\%$. The branching ratio of the available q^2 range has been obtained from the background
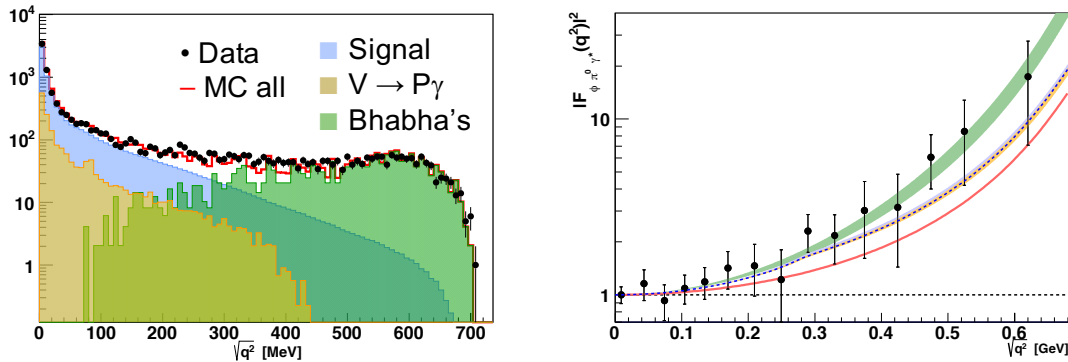

Figure 6: Analysis of the $\phi \to \pi^0 e^+ e^-$ decay channel. Left: data-MC comparison for the di-lepton invariant mass. Right: $\phi\pi^0$ form factor as a function of the di-lepton invariant mass. Predictions from dispersive analyses [7, 8] (orange, light blue, blue dashed), chiral theory approach [9] (green) and the one-pole VMD model (red) are also reported.

subtracted $e^+ e^-$ mass spectrum by applying an efficiency correction evaluated bin by bin:

$$BR(\phi \to \pi^0 e^+ e^-; \sqrt{q^2} < 700 \text{ MeV}) = (1.19 \pm 0.05^{+0.05}_{-0.10}) \times 10^{-5} \, . \tag{1}$$

The first error includes the statistical and normalization contributions, while the second one is due to systematics on analysis cuts and background subtraction. This result can be extrapolated to the full $\sqrt{q^2}$ range by using the theoretical description of the decay that best fits our transition form factor data [9]:

$$BR(\phi \to \pi^0 e^+ e^-) = (1.35 \pm 0.05^{+0.05}_{-0.10}) \times 10^{-5} \, . \tag{2}$$

The di-lepton invariant mass is reported in Fig. 6-right, after background subtraction and efficiency correction, and compared with theoretical predictions [7, 8, 9]. The slope of the transition form

factor has been extracted by fitting this curve in the one-pole approximation: $b_{\phi\pi^0} = (2.02 \pm 0.11)$ GeV^{-2}.

5.3 Precision measurement of the $\eta \to \pi^+\pi^-\pi^0$ Dalitz plot distribution with the KLOE detector

The $\eta \to \pi^+\pi^-\pi^0$ decay is fully dominated by the isospin violating part of the strong interactions. A high precision measurement of the $\eta \to \pi^+\pi^-\pi^0$ decay dynamics allows to access the light quark mass difference [10]. The Dalitz plot density is commonly described by a polinomial expansion in the X and Y variables:

$$|A(X,Y)|^2 \simeq N(1 + aY + bY^2 + cX + dX^2 + eXY + fY^3 + gX^2Y + hXY^2 + lX^3 + ...) \quad (3)$$

In 2008, the KLOE experiment measured for the first time the Dalitz Plot parameters up to the term f (KLOE08) [11]. These results have been recently confirmed, although with less precision, by the WASA and BESIII experiments [12, 13]. A new measurement has been performed with KLOE data (KLOE16), with an independent and ~ 4 times larger data set (1.7 fb^{-1}), a new analysis scheme and an improved Monte Carlo simulation, providing with improved accuracy the parameters of the decay matrix [3]. The resulting Dalitz plot density has been fitted, after background subtraction,

Table 1: Fit results for $\eta \to \pi^+\pi^-\pi^0$ Dalitz plot analysis, compared to previous KLOE results.

	a	b	d	f	g
KLOE08	$-1.090(5)(^{+8}_{-19})$	$0.124(6)(10)$	$0.057(6)(^{+7}_{-16})$	$0.14(1)(2)$	$-$
KLOE16	$-1.104(3)(2)$	$0.142(3)(^{+5}_{-4})$	$0.073(3)(^{+4}_{-3})$	$0.154(6)(^{+4}_{-5})$	$-$
KLOE16	$-1.095(3)(^{+3}_{-2})$	$0.145(3)(5)$	$0.081(3)(^{+6}_{-5})$	$0.141(7)(^{+7}_{-8})$	$-0.044(9)(^{+12}_{-13})$

with the complete third order polinomial expansion of Eq. (3), folded with smearing matrix and analysis efficency. Bin size is about three times the X, Y resolution. Fitting with the whole polinomial expansion, the c, e, h and l parameters are consistent with zero, as expected from C-invariance. Fixing them to zero and comparing with the previous KLOE measurement (Tab. 1), the statistical uncertainty is reduced by about a factor of two, while improving also the systematic uncertainties, which are in some cases reduced by a factor of $2 \div 3$. The major improvement in the systematic uncertainties comes from the analysis of the effect of the event classification with an unbiased prescaled data sample. When the g parameter is included in the fit, its value is different from zero at 3σ level, improving the χ^2 probability from 24% to 56%. Comparison of KLOE, WASA and BESIII shows a good agreement among experimental results, with KLOE16 being the most precise one. The unbinned integrated left-right (A_{LR}), quadrant (A_Q) and sextant

Table 2: Measurements of the charge asymmetries for $\eta \to \pi^+\pi^-\pi^0$.

Experiment	$A_{LR}(10^{-2})$	$A_Q(10^{-2})$	$A_S(10^{-2})$
Gormley68	1.5 ± 0.5	$-$	0.5 ± 0.5
Layter72	-0.05 ± 0.22	-0.07 ± 0.22	0.10 ± 0.22
Jane74	0.28 ± 0.26	-0.30 ± 0.25	0.20 ± 0.25
KLOE08	$0.09 \pm 0.10^{+0.09}_{-0.14}$	$-0.05 \pm 0.10^{+0.03}_{-0.05}$	$0.08 \pm 0.10^{+0.08}_{-0.13}$
KLOE16	$-0.050 \pm 0.045^{+0.05}_{-0.11}$	$0.020 \pm 0.045^{+0.048}_{-0.023}$	$0.004 \pm 0.045^{+0.033}_{-0.035}$

(A_S) charge asymmetries provide a more sensitive test of C parity conservation with respect to the fit to the Dalitz plot (Tab. 2). The values extracted from the analysis of the new KLOE data set are consistent with zero at 10^{-4} level, thus improving existent evaluations [14, 15, 16].

Systematic uncertainties are of the same size of the statistical ones except for A_{LR}, where the error is dominated by the description of the Bhabha background.

5.4 Measurement of the running of the fine structure constant below 1 GeV with the KLOE detector

Tests of the Standard Model and possible new physics deviations from it require the very precise knowledge of a set of input parameters, like the fine structure constant α, the Fermi constant G_μ and the Z boson mass M_Z. At zero momentum transfer, the electromagnetic coupling constant $\alpha(0)$ is very accurately known from the measurement of the anomalous magnetic moment of the electron and from solid-state physics measurements [17], $\alpha(0) = 137.035999084(51)[0.37\text{ppb}]$. In QED the coupling constant $\alpha(s)$ depends logarithmically on the energy scale due to the vacuum polarization.

We performed the measurement of the running of the QED coupling constant in the time-like region using the differential cross section $d\sigma(e^+e^- \to \mu^+\mu^-\gamma)/d\sqrt{s}$ in the energy range $0.6 < \sqrt{s} < 0.975$ GeV, with the photon emitted in the initial state [4]. The result shows a clear contribution of the $\rho - \omega$ resonances to the photon propagator with a significance of the hadronic contribution to the running of $\alpha(s)$ of more than $5\,\sigma$'s (Fig.7).
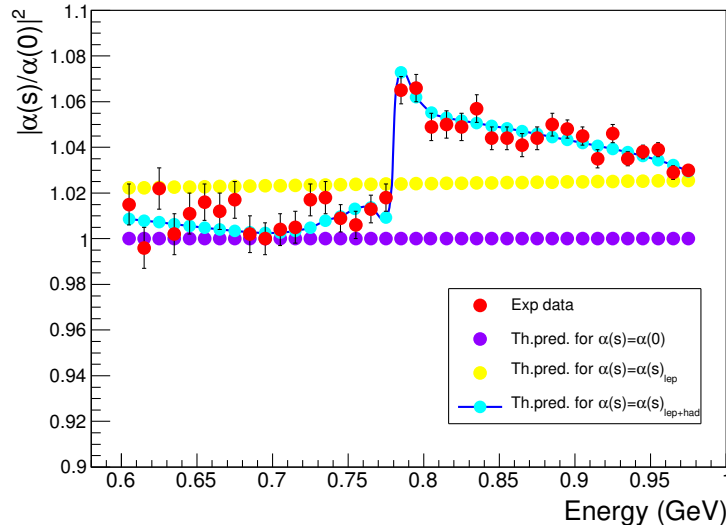

Figure 7: The square of the modulus of the running $\alpha(s)$ in units of $\alpha(0)$ compared with the `alphaQED` prediction [18] as a function of the dimuon invariant mass. The red dots are the KLOE data with statistical errors; the violet and yellow dots are the theoretical prediction for a fixed coupling and for only virtual lepton pairs contributing to the shift, respectively; the cyan dots with the solid line are the full QED prediction with both lepton and quark pairs contributing to the shift.

It represents the first measurement of the running of $\alpha(s)$ in this energy region and the strongest direct evidence achieved in both time- and space-like regions by a single experiment. For the first time the real and imaginary part of $\Delta\alpha(s)$ have been extracted, showing clearly the importance of the role of the second contribution (Fig.8).
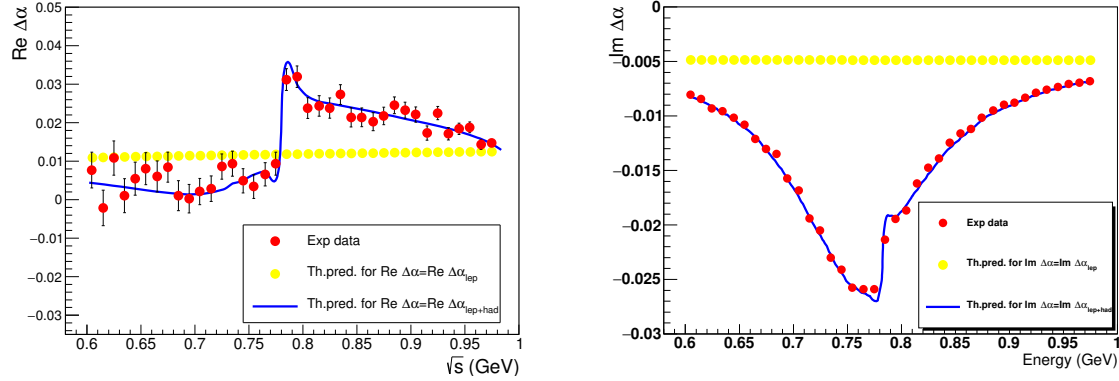
Figure 8: $\text{Re}\,\Delta\alpha$ (left) and $\text{Im}\,\Delta\alpha$ (right) extracted from KLOE data, compared with the `alphaQED` prediction (not including KLOE data) when considering virtual lepton pairs only (yellow points) and the full QED prediction (blue solid line).

From a fit to the real part of $\Delta\alpha(s)$ and assumming lepton universality, the branching ratio $BR(\omega \to \mu^+\mu^-) = (6.6 \pm 1.4_{\text{stat}} \pm 1.7_{\text{syst}}) \times 10^{-5}$ has also been obtained.

References

1. A. Anastasi et al., KLOE-2 Collaboration, Phys. Lett. B 757 (2016) 356–361

2. A. Anastasi et al., KLOE-2 Collaboration, Physics Letters B 757 (2016) 362–367

3. A. Anastasi et al., KLOE-2 Collaboration, JHEP 05 (2016) 019

4. A. Anastasi et al., KLOE-2 Collaboration, http://dx.doi.org/10.1016/j.physletb.2016.12.016.

5. S. Damjanovic *et al.*, Phys. Lett. B 677 (2009) 260.

6. D. Babusci *et al.*, Phys. Lett. **B 742** 1 (2015)

7. S. P. Schneider, B. Kubis, F. Niecknig, Phys. Rev. **D 86** 054013 (2012)

8. I. Danilkin *et al.*, Phys. Rev. **D 91** 094029 (2015)

9. S. Ivashyn, Prob. Atomic. Sci. Technol. **2012N1** 179 (2012)

10. H. Leutwyler, Mod. Ph. Lett. **A 28** 1360014 (2013) 1360014

11. F. Ambrosino *et al.*, JHEP **05** 006 (2008)

12. P. Adlarson *et al.*, Phys. Rev. **C 90** 045207 (2014)

13. M. Ablikim *et al.*, Phys. Rev. **D 92** 012014 (2015)

14. M. Gormley *et al.*, Phys. Rev. Lett. **21** 402 (1968)

15. J. G. Layter *et al.*, Phys. Rev. Lett. **29** 316 (1972)

16. M. R. Jane *et al.*, Phys. Lett. **B 48** 260 (1974)

17. T. Aoyama, M. Hayakawa, T. Kinoshita and M. Nio, Phys. Rev. D 77 (2008) 053012.

18. F. Jegerlehner, `alphaQED` package [version April 2012]
    `http://www-com.physik.hu-berlin.de/~fjeger/alphaQED.tar.gz`; see also F. Jegerlehner,
    Nuovo Cim. C **034S1** (2011) 31; Nucl. Phys. Proc. Suppl. **162** (2006) 22.